


# Super-Resolution-Chip: an *in-vitro* platform that enables super-resolution microscopy of co-cultures and 3D systems

OFIR SADE,<sup>1,6,†</sup> RONJA BONEBERG,<sup>2,7,†</sup> YIFAT WEISS,<sup>1,3,8</sup> MEGANE BELDJILALI-LABRO,<sup>2,9</sup> YAEL LEICHTMANN-BARDOOGO,<sup>2,10</sup> ITAY TALPIR,<sup>1,11</sup> IRIT GOTTFRIED,<sup>1,12</sup> URI ASHERY,<sup>1,3,13</sup> ROSSANA RAUTI,<sup>4,14,†</sup> AND BEN M. MAOZ<sup>2,3,5,15,†</sup> 

<sup>1</sup>*School of Neurobiology, Biochemistry and Biophysics, The George S. Wise Faculty of Life Sciences, Tel Aviv University, Tel Aviv, Israel*

<sup>2</sup>*Department of Biomedical Engineering, Tel Aviv University, Tel Aviv, 69978, Israel*

<sup>3</sup>*Sagol School of Neuroscience, Tel Aviv University, Tel Aviv, 69978, Israel*

<sup>4</sup>*Department of Biomolecular Sciences, University of Urbino Carlo Bo, Urbino, 61029, Italy*

<sup>5</sup>*The Center for Nanoscience and Nanotechnology, Tel Aviv University, Tel Aviv, 69978, Israel*

<sup>6</sup>*ofirsade@mail.tau.ac.il*

<sup>7</sup>*ronja.boneberg@uni-konstanz.de*

<sup>8</sup>*yifat354@gmail.com*

<sup>9</sup>*meganeb@mail.tau.ac.il*

<sup>10</sup>*ybardooogo@gmail.com*

<sup>11</sup>*t.itayt@gmail.com*

<sup>12</sup>*iritgot@gmail.com*

<sup>13</sup>*uriashery@gmail.com*

<sup>14</sup>*rossana.rauti@uniurb.it*

<sup>15</sup>*bmaoz@tauex.tau.ac.il*

<sup>†</sup>These authors equally contributed to this work

**Abstract:** The development of organs-on-a-chip platforms has revolutionized *in-vitro* cellular culture by allowing cells to be grown in an environment that better mimics human physiology. However, there is still a challenge in integrating those platforms with advanced imaging technology. This is extremely important when we want to study molecular changes and subcellular processes on the level of a single molecule using super-resolution microscopy (SRM), which has a resolution beyond the diffraction limit of light. Currently, existing platforms that include SRM have certain limitations, either as they only support 2D monocultures, without flow or as they demand a lot of production and handling. In this study, we developed a Super-Res-Chip platform, consisting of a 3D-printed chip and a porous membrane, that could be used to co-culture cells in close proximity either in 2D or in 3D while allowing SRM on both sides of the membrane. To demonstrate the functionality of the device, we co-cultured in endothelial and epithelial cells and used direct stochastic optical reconstruction microscopy (dSTORM) to investigate how glioblastoma cells affect the expression of the gap-junction protein Connexin43 in endothelial cells grown in 2D and in 3D. Cluster analysis of Connexin43 distribution revealed no difference in the number of clusters, their size, or radii, but did identify differences in their density. Furthermore, the spatial resolution was high also when the cells were imaged through the membrane (20-30 nm for x-y) and 10-20 nm when imaged directly both for 2D and 3D conditions. Overall, this chip allows to characterize of complex cellular processes on a molecular scale in an easy manner and improved the capacity for imaging in a single molecule resolution complex cellular organization.

© 2023 Optica Publishing Group under the terms of the [Optica Open Access Publishing Agreement](#)

## 1. Introduction

Recent years have seen an increased use and development of advanced *in vitro* models that better simulate human physiology. This is primarily due to the fact that such models allow us to better mimic cellular microenvironment (e.g., 3D structures, native extracellular matrix, co-culture, flow, etc. [1,2]), integrate sensors in complex cellular structures, and study organ-organ and systemic interactions. While these advanced *in vitro* models significantly developed over the past decade [3], extracting information about tissue state, or functionality still remains challenging. In recent studies, different sensors (like multielectrode arrays [4], transepithelial electrical resistance [5], mass spectrometer, oxygen, pH, and more) [6] have been integrated; however, they lack the ability to have spatial information of protein distribution, in a quantitative way and at the protein level.

It is important to note that imaging at the molecular scale, thus resolving subcellular structures and detecting molecular changes in protein distribution, requires resolution below the microscope's diffraction limit. This can be achieved by a series of techniques, collectively known as super-resolution microscopy (SRM). State-of-the-art SRM tools such as Stimulated Emission Depletion (STED) Microscopy, Photoactivated Localization Microscopy (PALM) and direct Stochastic Optical Resolution Microscopy (dSTORM) provide high lateral and axial resolutions of 10-20 nanometers [7], and recently also reached the nanometer level [8]. While these tools enable imaging of cellular morphology, protein organization, and sub-cellular structures, they require precise platforms for sample imaging, and they are limited to a short working distance of approximately 170  $\mu\text{m}$  imposed by objectives with a high numerical aperture (NA). Because of this limitation, samples that are imaged with SRM are relatively thin unless they are imaged using a demanding microscopy technique such as Lattice Light Sheet Microscopy optimized with Adaptive Optics [9]. Because this technique is so restrictive in the type of samples which can be imaged, samples and methods such as 3D samples, Organs-on-a-Chip, microfluidics, and 3D co-cultures are extremely challenging to image [10].

Different methods were developed to allow the use of SRM with advanced *in-vitro* models. A couple of examples are the work of Chu *et al.* [11], and Tam *et al.* [12], who used SRM with microfluidic platforms; however, their work is still limited to monocultures and a monolayer of cells grown on coverslips in a 2D environment. More advanced systems were developed to allow the co-culturing of cells with SRM, but in addition to its complex design and demanding manufacture [13], the system has a very small imaging area (170 x 170  $\mu\text{m}$ ), and is limited to 2D samples (which are cultured on a custom membrane made *via* multiphoton lithography). Recently, two platforms were developed to use SRM with 3D-cultures [14,15]. Despite providing a new concept for using SRM for non-planar (2D) samples, these platforms are specifically designed for 3D systems and are not compatible with Organs-on-a-Chip, microfluidics, and co-culture grown on a membrane.

In this work, we developed a Super-Res-Chip (Fig. 1) that allows the use of SRM with advanced *in vitro* systems, such as Organs-on-a-Chip, co-cultures, and 3D systems which can be compatible with standard well-plates. Moreover, the sample is held by a special holder which can be flipped, and by this, it increases the depth that can be imaged by the SRM. It is important to note that the Super-Res-Chip is fabricated using a 3D printer, making fabrication cheap and easy and enabling other labs to easily adapt it to their needs. This makes the Super-Res-Chip not only modular, but also very simple to apply in any standard well-plate.

To demonstrate the capabilities of the system, we co-cultured vascular endothelial Human Umbilical Vein Endothelial Cells (HUVEC) on a membrane and in a 3D gel with U87 glioblastoma cells, and then used SRM to monitor the differences in expression of the gap junction protein Connexin43 (Cx43) by endothelial cells when cultured under different microenvironments (2D monoculture, co-culture on a membrane and co-culture in 3D). Gap junctions are intercellular membrane channels produced between adjacent cells. Both glioma cells and HUVEC form gap

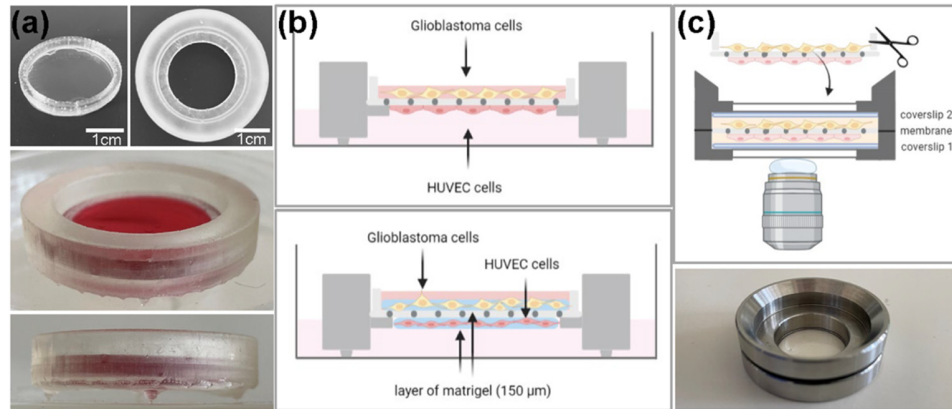


**Fig. 1. Schematic of the Super-Res-Chip System.** (a) Building blocks of the Chip: PDMS-ring with PC-membrane (left) and 3D-printed Chip (right); top- and side-view of the assembled platform. (b) Scheme of the co-culture in the chip: U87 glioblastoma cells cultured on the upper side, together with HUVEC cells on the bottom side of the membrane either directly on the membrane (top) or in a layer of Matrigel (approx. 150 $\mu$ m). (c) Principle of dSTORM imaging of the membrane: The PDMS ring is cut off, the membrane inserted into the Attofluor cell chamber in between two round glass coverslips, together with imaging buffer (top). Attofluor cell chamber for microscopy of the membranes (bottom). Schemes in (b) and (c) were created with BioRender.com.

junctions, with Cx43 being one of the primary proteins expressed [16,17]. Communication between glioma cells and HUVECs as well as between the HUVEC themselves occurs through gap junctions [16], with Cx43 shown to be necessary for their functional formation. These junctions can thus play a critical role in regulating cell growth, differentiation, and morphogenesis. Moreover, tumor angiogenesis is a complex process based upon a sequence of interactions between tumor cells and endothelial cells [18]. In view of this, it is crucial to develop platforms with the potential to monitor cell-cell interactions at the molecular level and to offer a biological model system that will give new insight into the biology of tumor progression.

Overall, with our system, we demonstrated that the microenvironment influences cellular morphology [18–21] and the use of SRM improved the identification and characterization of proteins in advanced *in-vitro* systems based on their spatial distribution. This novel platform, able to image and measure cell-cell interactions at a molecular level, will give the opportunity to advance knowledge of these phenomena and to enable high-throughput screening and drug discovery with time and cost benefits.

## 2. Methodology

### 2.1. Super-Res-Chip fabrication and assembly

The Super-Res-Chips were designed using SolidWorks CAD software and printed with dental long-term clear resin (RS-F2-DLCL-01, Formlabs, Somerville, Massachusetts) using a stereolithography printer (Form2 3D printer, Formlabs). After printing, the chips were washed with isopropyl alcohol in an ultrasonic bath and subsequently cured and dried in a UV curing system [22]. These chips had the following dimensions: an internal diameter of 29 mm, an external diameter of 40 mm, a height of 9 mm, with 2 mm high legs (Fig. 1(a)), and a supporting ring of 2 mm wide and 3 mm high. The master molds for the fabrication of the polydimethylsiloxane (PDMS) support rings were designed with the SolidWorks CAD software. The molds were printed using a Raise 3D Pro2 Dual Extruder 3D Printer (Raise Technologies, Inc.) with a commercial polylactic

acid filament. After that, the molds were filled with PDMS made from Sylgard 184 mixed with the curing agent in a 1:10 ratio, then cured overnight at 60°C. The resulting PDMS rings were cleaned in ethanol, dried at room temperature (RT), and subsequently activated by oxygen plasma treatment (Atto-BR-200-PCCE, Diener Electronic, Germany) for 30 s. Polycarbonate membranes (pore size: 0.4µm, it4ip S.A., Belgium), 25µm thick, were cut to an according size, washed with isopropanol, dried at RT, and activated by plasma treatment for 60 seconds. Afterward, membranes were immersed in a 5% aqueous solution of 3-aminopropyltriethoxysilane (APTES, 440140 Sigma-Aldrich) for 30 minutes, rinsed with H<sub>2</sub>O, and dried under a stream of compressed air. Membranes and PDMS-rings were aligned and gently stuck together before they were heated in the oven at 60°C overnight. Before use, membranes were washed with 70% ethanol three times, washed with PBS four times, dried and sterilized with UV light for 30 minutes. Chips were incubated in 70% ethanol for 30 minutes prior to sterilization with UV. After seeding cells, membranes assembled with the PDMS rings were inserted into 3D-printed Super-Res-Chips.

## 2.2. Cell culture

Endothelial and glioblastoma cells were used for single and co-cultures in the chip system. Primary Human Umbilical Vein Endothelial Cells (HUVEC, C-12200 PromoCell GmbH, Heidelberg, Germany) were cultured in low-serum endothelial cell growth medium (C-22110, PromoCell) at 37°C, with 5% CO<sub>2</sub> in a humidifying incubator. Passages p4-p7 were used for all experiments. The cancer cell line U87 glioblastoma (ATCC) was grown in low-glucose Dulbecco's Modified Eagle's Medium (DMEM, 01-055-1A Biological Industries) supplied with 10% FBS (04-001-1A, Biological Industries), 1% PenStrep (03-031-1B, Biological Industries) and 1% Glutamax (35050061, Gibco) at 37°C with 5% CO<sub>2</sub> in a humidifying incubator. Seeding was performed after both cell types had reached 90% confluence [22].

## 2.3. Cell seeding

Endothelial and glioblastoma cells were cultured separately on one side of a chip membrane, as well as co-cultured on the two sides of the membrane. First, endothelial cells were seeded on the bottom side of the membrane and incubated overnight, followed by glioblastoma cells seeded on the upper side. Before seeding the HUVEC cells, membranes were coated with Entactin-Collagen IV-Laminin (ECL) Cell Attachment Matrix (08-110, Merck) diluted 1:100 in DMEM for 1 h at 37°C. Then HUVEC cells were harvested using Trypsin EDTA solution B (03-052-1A, Biological Industries) and seeded onto the membrane at a density of 40,000 cells/cm<sup>2</sup>. Following the cell adhesion for about 2 h, the membranes were flipped and inserted into the Super-Res-Chips along with medium.

In the next day, the other side of the membrane was coated with Matrigel Basement Membrane Matrix (354262, Corning, diluted 1:50 in DMEM) for 1 h at 37°C. U87 glioblastoma cells were also harvested with Trypsin/ EDTA and seeded in a density of 40,000 cells/cm<sup>2</sup>.

Seeded cells were co-cultured for 48 h before being fixed.

For the culture of the cells in a layer of matrigel with a height of approximately 150 µm, 74 µL of a 1:1 mixture of cell suspension and matrigel was applied to each side of the membrane. Then, both cell lines were seeded using the same procedure described before.

## 2.4. Fixation and immunostaining

In order to fix the cells, we removed the membrane from the chip using tweezers holding the PDMS ring, and then transferred it to a 6-well plate.

HUVEC and cancer cell lines were rinsed in PBS four times and fixed by incubation with 4% paraformaldehyde (PFA, 158127 Sigma-Aldrich) for 20 minutes at RT. Subsequently, to remove residual PFA, cells were washed with PBS for 5 minutes three times. For permeabilizing cell membranes, 0.1% TritonX-100 (T8787 Sigma-Aldrich) was added to PBS and incubated for 10

minutes at RT. Cells were then washed three times with PBS, followed by blocking with PBS containing 5% goat serum and 0.1% BSA for 1 h at RT. Primary antibodies (mouse anti- $\beta$ -tubulin III, 1:300, Abcam 78078, anti-rabbit Cx43, 1:500, Abcam, #ab11370; anti-rabbit CD31, 1:250, Abcam, #ab28364) diluted in blocking solution were applied overnight at 4°C. After washing three times with PBS, the cells were incubated with the secondary antibodies (anti-mouse Alexa Fluor 647, 1:500, Abcam ab150115, anti-rabbit Alexa Fluor 594, 1:500, rhenium A11012, and goat anti-rabbit CF568, 1:500, Biotium #20801) for 45 min. After four washes with PBS, cells were incubated with Hoechst 33342 (Invitrogen, 1:200 dilution) in PBS for 10 minutes at RT to stain the nuclei. The cells were then washed with PBS three times and kept in PBS solution at 4°C until imaging.

### 2.5. Imaging

Fluorescence imaging was performed using an inverted confocal microscope (Olympus FV3000-IX83) and a single-molecule localization microscope (Vutara 350, Bruker). Confocal imaging was performed by placing the membrane on a glass slide, using tweezers holding the PDMS ring. Imaging was carried out using a confocal microscope with suitable filter cubes and equipped with 20x (0.8 NA) and 40x (0.95 NA) lens objectives. Confocal measurements were performed using laser 405 nm, at 0.5% laser transmissivity, PMT voltage 640 V and laser 561 nm, at 2.5% laser transmissivity, PMT voltage 686 V. Pinhole (confocal aperture) was of 180 $\mu$ m. The image size was 512  $\times$  512 pixels, 318.198 $\mu$ m  $\times$  318.198 $\mu$ m. The pixel size was 0.6215 $\mu$ m/pixel.

dSTORM imaging was performed after removing the PDMS ring and the membrane was fixed in the Attofluor cell chamber in between two coverslips. Before being used, the coverslips were cleaned by autoclave, ethanol 70% and UV light. To enable single-molecule photoswitching of the dyes Alexa Fluor 647 and CF 568, the chamber was filled with imaging buffer B (50 mM Tris-HCl pH 8, 10 mM NaCl, 10% (w/v) glucose) supplemented with 20 mM cysteamine (MEA; dissolved in buffer A (50 mM Tris-HCl pH 8, 10 mM NaCl)), 2% (v/v) glucose oxidase (168.8 AU) and catalase (1404 AU) mixture in buffer A and 1% (v/v) 2-mercaptoethanol. Image processing was carried out using the open-source software ImageJ and home-written analysis software.

### 2.6. Super-resolution acquisition

Direct Stochastic Optical Reconstruction Microscopy (dSTORM), super-resolution imaging was done using a single-molecule localization microscope (Vutara 350, Bruker). A movie showing raw localization and blinking is presented as supplementary data ([Visualization 1](#)). We used 561 nm and 647 nm lasers with power of 1000 mW. The range of capabilities of our system are 5-10 kW/cm<sup>2</sup>. In this study, 30% laser power was applied so that would mean approximately 1.5-3 kW/cm<sup>2</sup>. A pentaband dichroic mirror and emissions filters were used throughout the study [23].

The manufacturer Vutara 350's defined precision is: 20 nm XY and 50 nm Z resolution. The actual microscope's lateral resolution ranges between 15 nm – 40 nm and its axial resolution ranges between 50 nm – 80 nm. It's important to state that we were not using Z-stack imaging, since we were imaging the sample at one Z plane.

The Vutara350's custom case is designed for super-resolution, environmental isolation, temperature regulation, and drift minimization. The z-step between planes in the software is set to 100 nm. To estimate the drift in our system we imaged 100 nm TetraSpeck beads for 2000 frames (equivalent to the samples' imaging), with 30% laser power, and examine the localization precision. We found a slight drift in some scans of 10-30 nm. Therefore, our minimal XY spatial precision is 30 nm (Supplementary Figure 1 in [Supplement 1](#)). Moreover, to measure spherical aberration, we imaged 100 nm Tetraspeck beads over 12  $\mu$ m and examined the localization precision. In each plane a bead was fitted with a point spread function (PSF); the PSFs at depths

0-90  $\mu\text{m}$  are similar, and the PSF at 125  $\mu\text{m}$  depth is slightly wider (Supplementary Figure 2 in Supplement 1). It's important to note that while there is a slight difference, localizations with wide PSFs are dropped by the Vutara SRX software automatically. As all the localizations in our study were accepted by the software, according to Bruker, it means that they were well-fitted and the precision represents a real value.

Localization-based super-resolution microscopy like dSTORM, provides spatial resolution of 10-30 nm. This was shown to be the case in many publications, yet imaging through a 3D gel or through the membrane might reduce the localization accuracy. We used a built-in feature in Bruker's software (Vutara SRX), the practical localization accuracy measure (PLAM) [24–26] that provides a lower bound on the accuracy with which an unknown parameter like a single molecule is estimated when imaged using a pixelated detector. The PLAM was calculated using the Cram'er-Rao lower bound, that is, the inverse of the Fisher information [27] which represents the amount of information provided by the data about an unknown parameter.

The Bruker patented Biplane technology offers higher localization accuracy than astigmatism over a larger axial range, and therefore it is the preferred commercial 3D super-resolution method. Compared to astigmatism, Biplane offers superior localization due to its enhanced per-pixel SNR. By detecting the PSF on two different focal planes, and summing the photon count over an expanded axial range (without the perceived loss of photons), the Biplane and Quadfield modules yield superior localization precision in the z plane [28].

The cameras used are a sCMOS camera (4 MP, 6.5  $\mu\text{m}$  x 6.5  $\mu\text{m}$  pixel size for super-resolution imaging) and a CCD camera (1392 x 1040 for widefield imaging).

All imaging was done using water immersion 60x objective (1.20 NA), on a field of view of 10  $\mu\text{m}$  x 10  $\mu\text{m}$ .

## 2.7. Cluster analysis

For each condition, 10 dSTORM images of four independent replicates were randomly taken. A density-based clustering algorithm, Hierarchical Density-Based Spatial Clustering of Applications with Noise (HDBSCAN) [29], was used to analyze the localizations extracted from each image. We used an existing implementation from the Python library "HDBSCAN-clustering". HDBSCAN determines the core-distances for each localization to estimate its probability density function (PDF). The core-distance of a point is its distance from its  $k^{\text{th}}$  nearest neighbor; the denser the area, the smaller the core-distance of a point is. The parameters we used were: minPoints = 50, and the extracting algorithm was 'leaf'. HDBSCAN supports a parameter that determines how it selects clusters from the hierarchical cluster tree. 'Leaf' clustering directs HDBSCAN to select leaf nodes from the tree, producing many small homogenous clusters while still allowing clusters that vary in size and density. Nevertheless, using 'leaf' extraction will result in a tendency to produce a more fine-grained clustering than other available methods [30].

We applied 30% denoise using the "Mean Distance" algorithm in Vutara SRX, as well as noise-reduction with Principal Component Analysis (PCA) with a standard deviation of 1.0. The PDF of a point is defined as the probability of being within a small region around it, and can also be interpreted as the expected density around that point. Based on the mutual reachability distance, HDBSCAN assigns points to the clusters. The mutual reachability distance of a pair of points is the maximum value between the core-distance of point 'a', the core-distance of point 'b' and the distance between points 'a' and 'b'. Localizations of Connexin43 proteins in the dSTORM images were extracted as xy-coordinates and analyzed for cluster size, density and number of localization per cluster. It is important also to note, that for our cluster analysis, we took into consideration fluorophore properties. Indeed, fluorophores may stay in the "on" state for a time period of tens of milliseconds. Accordingly, fluorophores that were detected within 1 pixel (96 nm) of each other in up to 3 consecutive frames (frame duration is set to 20 ms each,

with 20 ms between frames, a total of 120 ms for 3 frames, allowing fluorophores to turn on and off within the timeframe of 3 frames) were accumulated into one localization.

### 2.8. Statistical analysis

The results are presented as mean  $\pm$  SEM. Statistically significant differences among two different groups were evaluated either by multiple t-test for each bin in the histograms without assuming the same Standard Deviation (SD; GraphPad Prism 8.0.1). A statistically significant difference between two data sets was assessed and  $P < 0.05$  was considered statistically significant.

## 3. Results and discussion

### 3.1. Super-Res-Chip system

The primary goal of this work was to develop a modular, easy-to-fabricate, and use “Chip” system that will allow the use of SRM with complex tissues (e.g. 3D, Organs-on-a-Chip, etc.). To do so, we designed a special Chip based on that developed by Rauti *et al.* [22]. Differently from that, the chip has bigger dimensions in order to fit inside the *d*STORM imaging chamber and it doesn't have inlet and outlet openings since no microfluidic experiments were needed for the purpose of this study.

Using this special Chip, cells are grown on a flat permeable membrane, allowing them to be seeded from both sides and examine the effects of one cell type on the other. When creating a chip system that could be integrated with imaging platforms, such as confocal or SRM, the first challenge is to ensure that the membranes remain flat during the culture, fixation, and imaging processes, in order to avoid imaging artifacts or cell-damaging, but on the other hand, the system must be modular, removable, and can be used with multiple setups.

Figure 1 shows the main components and features of the Super-Res-Chip. This device is 3D-printed from clear dental resin and contains a cell culture chamber with an internal diameter of 29 mm and an external diameter of 40 mm, with a capacity of up to 4 mL of cellular medium. The Chip stands on four short legs (2 mm high) and thus can stand alone in a well-plate, thereby enabling medium change and the ability to also co-culture either on the porous membrane or on the bottom of the well into which the Chip is inserted (Fig. 1(a), **bottom panel and 1b**).

A PDMS-ring (2 mm width and a 3 mm height) was coupled with a poly-carbonate membrane (inner diameter of 24 mm, pore size of 0.4  $\mu$ m), allowing the diffusion between the different cell types co-cultured on either side (Fig. 1(a), **left panel**). It is important to note that the size of the Super-Res-Chip System was chosen in order to fit inside the *d*STORM imaging chamber (Fig. 1(c)), but it can be adjusted per device.

In order to show the applicability and importance of the microenvironment to cellular growth together with SRM, we cultured endothelial (HUVEC) and epithelial (U87 glioblastoma) cells under three different conditions: monoculture, co-culture on a membrane, and co-culture in 3D (Fig. 1(b)). We studied and characterized the morphological changes and protein expression using different imaging methods (confocal and *d*STORM).

### 3.2. Super-Resolution Imaging of the Super-Res-Chip Membrane

The modularity of the chip allows to disconnect the sample from the chip (Fig. 1(c)) and to use a number of imaging techniques, such as confocal and SRM (Figs. 2, 3). It is well known that the cellular properties are influenced significantly by the culture conditions and cellular microenvironment [31]. Figure 2 and (Visualization 2 shows the confocal images of HUVEC and U87 as monocultures and co-cultures (on both sides of a membrane). It can be seen, that both cells express the expected proteins (Cx43 for the HUVEC and  $\beta$ -III-tubulin for the U87).

As a next step, we took the same samples that were imaged by the confocal microscope, to the *d*STORM for SRM. Through *d*STORM, we were able to investigate the distribution of proteins

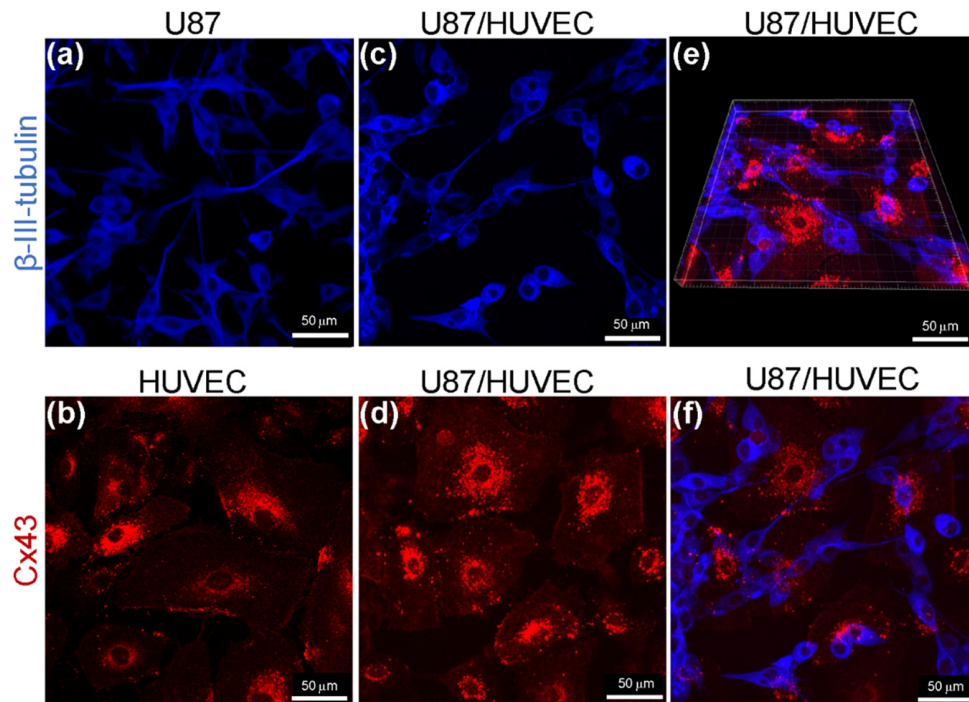


**Fig. 2. Confocal images of U87 and HUVEC grown in the chip.** (a) Confocal reconstruction of U87 glioblastoma monoculture stained for  $\beta$ -III-tubulin (blue; goat anti-rabbit CF568); (b) confocal reconstruction of HUVEC monoculture stained for Connexin43 (red; goat anti-mouse Alexa Fluor 647); (c,d) confocal reconstruction of HUVEC/U87 co-culture with (c) U87 stained for  $\beta$ -III-tubulin and (d) HUVEC stained for Cx43, (e) 3D-reconstruction of images (c) and (d) with U87 on top and HUVEC on the bottom, (f) merge of images (c) and (d) in 2D.

on a single molecular level and so, the possible effects of growing HUVEC and U87 in close proximity on Cx43 distribution.

Figure 3, shows representative widefield and super-resolution images of the cells that were growing on our Super-Res-Chip. Super-resolution images of U87 cells revealed the typical tubular structure of microtubules (Fig. 3(a) and (d)), and it also allowed us to image the tubular spindles of cells undergoing mitosis (Fig. 3(d)). Cx43 is a gap junction protein that allows gap junctions to regulate the passage of small molecules and ions between cells [32]. Imaging of Cx43 in HUVEC cells with SRM revealed Cx43 distribution at the plasma membrane between adjacent cells (Figs. 3(b), 5) [33,34]. According to *d*STORM images, Cx43 is distributed in clusters of various shapes and sizes (Fig. 3(c) and (f)) and we can calculate the number of Cx43 molecules in each cluster as the size and density of each cluster (Fig. 5, bottom panel). Taking advantage of the permeable membrane by co-culturing HUVEC cells on one side and U87 cells on the other side of the membrane, allows us to investigate the possible influence of U87 cells on the distribution of Cx43 in HUVEC cells. As can be seen in Fig. 3(e) and 3(f), Cx43 clusters are still detected at the plasma membrane of adjacent cells with different shapes, ranging from small dots to long dash-like structures, similar to HUVEC cells grown alone (compare Fig. 3(b), (e) and the relative higher magnification 3(c) and 3(f)).

In order to assess the precision of the system and if it is reduced in 3D or when we imaged through the membrane, we used PLAM [24–27] (Fig. 4) which enables to quantify the resolution



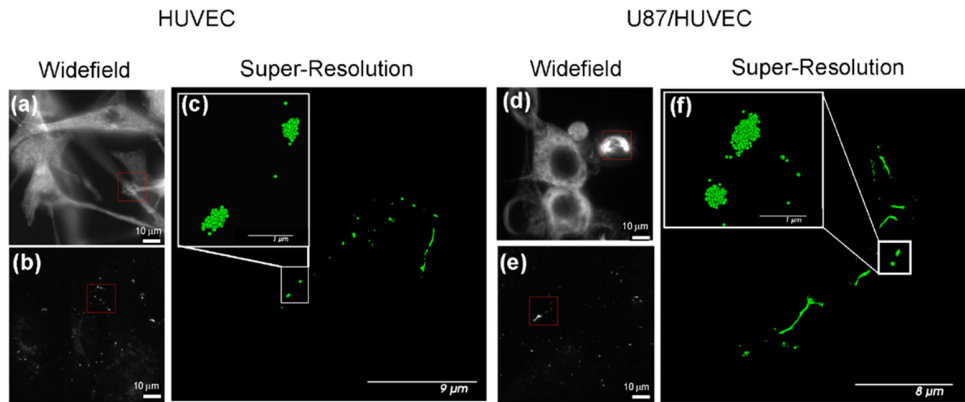


**Fig. 3.** shows representative widefield and super-resolution images of the cells that were growing on our Super-Res-Chip. Super-resolution images of U87 cells revealed the typical insert) Higher magnification of Cx43 clusters in HUVEC grown alone show Cx43 clusters; (d, e) Conventional widefield images of microtubules (d) and Cx43 (e) in HUVEC cells grown with U87 cells. (f) Super-resolution image of Cx43 (green) in HUVEC cells grown with U87 cells shows puncta staining. (f, insert) Higher magnification of Cx43 clusters in HUVEC cells grown with U87 cells x43 clusters.

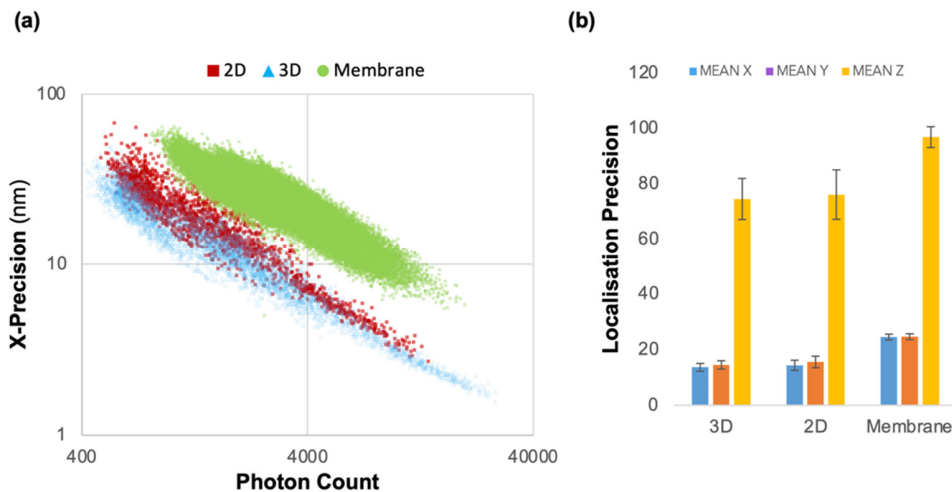


**Fig. 4. Resolution precision of the Super-Res-Chip System.** (a) scatter plot of the correlation between the photon count and the localization precision on the x-axis, in 2D (blue squares), 3D (purple triangles), and on membrane (green circles; plots are on a log-log scale); (b) Bar plot of the mean localization precision of each axis (x,y,z) in 3D, 2D and on membrane samples (**3D**: Mean X = 13.653, Mean Y = 14.512, Mean Z = 74.544; **2D**: Mean X = 14.387, Mean Y = 15.586, Mean Z = 76.124; **Membrane**: Mean X = 24.538, Mean Y = 24.650, Mean Z = 96.851. Bars represent standard error of the mean.

precision in each one of the axis. As shown in Fig. 4, for all 3 conditions (2D monoculture, 3D, and membrane), the correlation between the photon count for each localization and the localization precision demonstrates that the resolution precision for each localization was improved at higher photon count (Fig. 4(a)), reflecting better PSF fitting. In addition, all 3 conditions (2D, 3D, and membrane), have a single molecule, high resolution precision in the x and y axis (10-20 nm in 2D and 3D and 20-30 nm with membrane) and as expected, lower resolution in the z axis

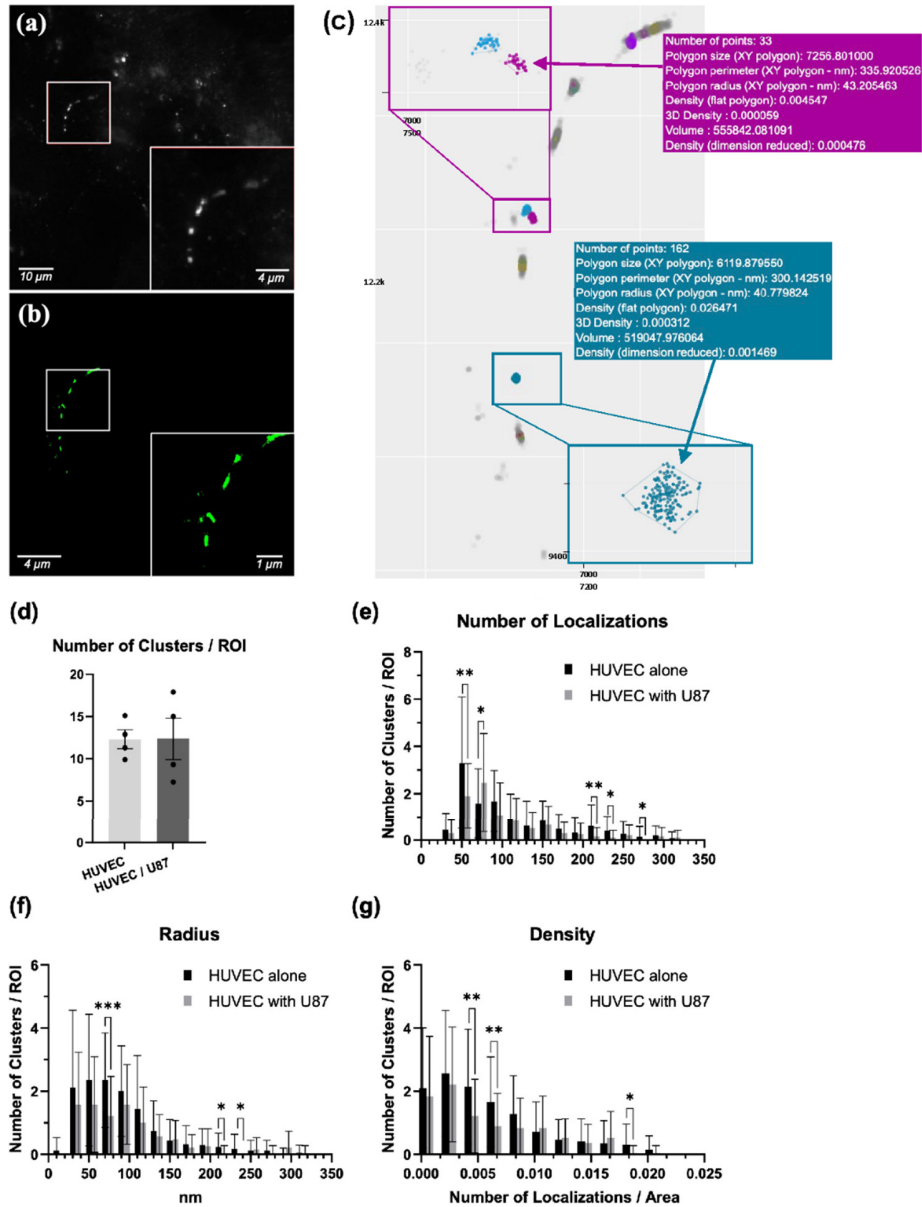


**Fig. 5. HDBSCAN analysis of Cx43 clusters in HUVEC cells grown alone or co-cultured with U87 cells.** (a) Representative wide-field low resolution image of Cx43 staining in HUVEC cells. (b) dSTORM image of the selected area reconstructed from single-molecule localizations. (c) Examples of clusters recognized by a density-based algorithm of the same region. Inserts show inner structure and parameters of several Cx43 clusters showing the number of localizations/molecules, clusters' radius and density. Comparison of the number of Cx43 clusters was significantly different when HUVEC cells were co-cultured with U87 cells. Each color represents a different cluster. (d). Similarly, the distribution of number of localizations per cluster (e), cluster radii (f) and cluster densities (g) were affected by U87 cells. Data is shown as  $\pm$  SEM from  $N = 4$  (with 10 technical replicates each) (d) or as frequency distribution of  $N = 4$  (f-g). Statistical significance was analyzed by multiple t-test (\* =  $P \leq 0.05$ ; \*\* =  $P \leq 0.01$ ; \*\*\* =  $P \leq 0.001$ ).

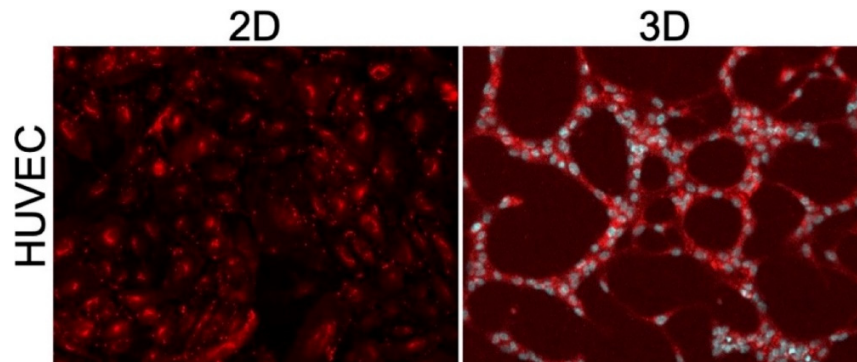


**Fig. 6.** Morphological differences of cells grown in 2D and 3D. (a) Comparison of HUVEC cells grown on a coated membrane with growing them in a layer of Matrigel, stained for CD31 (red, anti-rabbit Alexa Fluor 594).

(70-80 nm in 2D and 3D and 80-100 nm with membrane). We found it encouraging for future studies that imaging in 3D gel do not reduce the resolution precision while imaging through a porous membrane reduces resolution precision most probably due to light scattering through the membrane, yet the single molecule resolution with a 20-30 nm resolution precision allow quantification of protein organization with high precision.

In order to measure the effect of co-culturing HUVEC cells with U87 cells, we quantified the organization of Cx43 using a clustering algorithm called Hierarchical Density-Based Spatial Clustering of Applications with Noise (HDBSCAN) [29] (Fig. 5).

It determines the core-distances for each localization to estimate its probability density function (PDF). Based on the mutual reachability distance, it connects points to different clusters. As one can see, the analysis provides not only the number of clusters in each image, but also provides cluster characteristics such as their number of Cx43 molecules (localizations), radius (in nm), and density (Fig. 5). The density is defined as the number of localizations per area of the cluster, which is calculated using its convex hull.

We compared all different Cx43 cluster characteristics detected by HDBSCAN for HUVEC cells cultured alone with HUVEC cells co-cultured with the U87. Figure 5 (bottom panel) shows the results for the number of clusters per imaged region of interest (ROI) and the distribution of the number of localizations, radii, and densities for each cluster that was identified. The results of the technical replicates of every membrane were averaged and combined. The number of clusters for both culture conditions accounts for an average of 12.2 ( $\pm$  SEM for each condition) clusters per ROI. We then analyzed the number of localizations per cluster and displayed it in a histogram that shows that most clusters include about 50 to 70 molecules/localizations, and, as expected the distribution was mainly similar for both HUVEC cells cultured alone or and co-cultured with U87 cells, with few points showing some significant changes.

The distribution of the cluster radii ranging mostly from about 30 to 110 nm, showed a significant change when comparing HUVEC alone and co-cultured with U87. It is important to note, that during our statistical tests we took in consideration the overlap of some error bars, probably due to the variability of the measurements probably related to the complexity of the cellular mechanisms underlying these cellular interactions.

Indeed, this is in line with what was previously reported in the literature, where changes in HUVEC Cx43's expression could be seen when cells are cultured at different densities [16].

### 3.3. 3D culture of cells in matrigel

After demonstrating that the Super-Res-Chip could image cells grown on two sides of a membrane, we used the system to demonstrate its capabilities to image 3D systems with SRM, such as co-culture in 3D gels. To do so, we cultured the HUVEC in a 3D gel with a total height of about 300  $\mu\text{m}$ . As expected, cells that were cultured in 3D display a different morphology compared to cells grown in 2D (Fig. 6 and Supplementary Figure 3 in Supplement 1).

The confocal imaging reveals that when cultured directly on the membrane, endothelial cells form a confluent monolayer (Fig. 2), whereas when cultured in a 3D gel, they form tubular structures (Fig. 6(a)). The tubular organization was most easily detected through the combination of Cx43 and Hoechst staining of cell nuclei (Supplementary Figure 3 in Supplement 1). Furthermore, we used the Super-Res-Chip for super-resolution imaging of the 3D system as

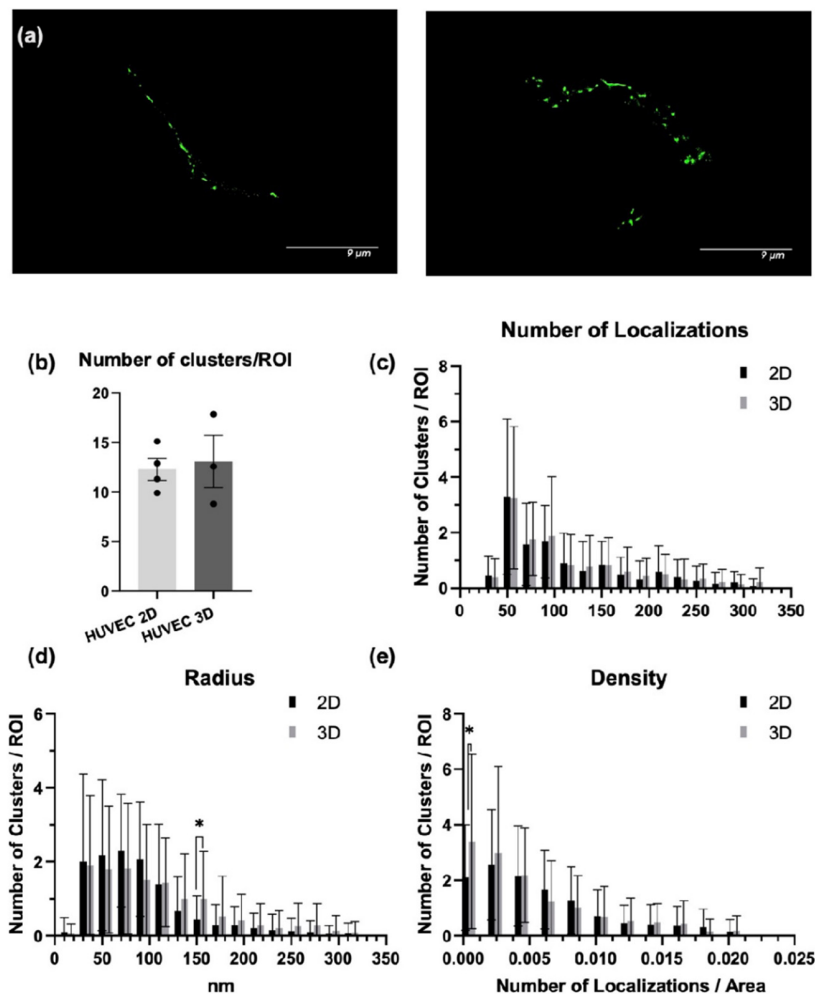


**Fig. 7.** Cx43's cluster analysis show differences between cells grown in 2D and 3D. (a) SRM images of HUVEC cells grown on a coated membrane with growing them in a layer of matrigel (upper panel). Cluster characteristics that were analyzed were the number of Cx43 clusters (b), the distribution of number of localizations per cluster (c), cluster radii (d) and cluster densities (e). Statistical significance was analyzed by multiple t-test). No significant differences between the groups were found in the above parameters.

described in Fig. 1(c), which allowed us to image up to 300 $\mu$ m (150 $\mu$ m on each side, by flipping the sample). Interestingly, the *d*STORM data (Fig. 6) showed that despite the morphology of endothelial cells changed significantly when they were cultured in 3D, the CX43 clusters look quite similar between the 2D and 3D samples (Fig. 5).

We next quantified the Cx43 cluster's parameters. As shown in Fig. 7, the number of clusters per ROI, number of localizations per cluster, cluster radii, and densities did not change significantly between the 2D and the 3D samples, except for the low number of cluster densities. Interestingly, we can see that the HUVEC organization is clearly morphologically different in the 3D environment, compared to the 2D, implying that there are significant changes in other proteins other than Cx43. Aside from this, at the time we measured the effects of co-culturing U87 with HUVEC cells, we found that there was no effect on the organization of Cx43, as we expected or that the gap junction is not affected by the time that they were co-cultured. In fact, changes in the cellular properties were observed after 14 or 21 days of co-culturing [35] or when U87 cells were plated at much higher densities [18]. It is important to note that there are not many studies that looked at the communication of such cell lines with HUVEC. To our knowledge, the only evidence of such interactions has been found by Thuringer *et al.*, who found that heat shock protein HSP27 secreted by the colorectal cancer cell line SW480 increased the communication of neighboring endothelial cells measured by fluorescence recovery [36]. However, increased communication does not necessarily require a higher number of gap junctions, as we investigated in this study. We must keep in mind, however, that although the exact mechanism by which proteins change as a result of co-culture and change in the microenvironment has still to be identified, our work provides a new platform that enables advanced *in vitro* tools to be used with SRM, in order to extract spatial information with a 20 nm resolution.

#### 4. Conclusion

Overall, we were able to design and implement a new platform, which allows advanced *in vitro* models to be used with SRM technology. Designed to fit any standard well-plate, the system is easy to fabricate using a 3D printer, and it can also be used for a variety of applications and microscopes (including confocal and *d*STORM). In this work, we used our platform to demonstrate the importance of using an “*in-vivo* like” microenvironment, which includes multiple cell types and a 3D environment, as well as to characterize the changes in the protein expression. By using our new system, we were able to multiply the imaging depth (from 200  $\mu$ m to 300  $\mu$ m) and image different platforms (Organs-on-a-Chip, 3D gels, etc). Overall, we were able to observe significant morphological changes when cells were cultured in 2D compared to 3D systems, and some minor differences in the expression of Cx43, as a result of the duration the co-culturing process, obtaining similar results to some already published works.

Considering the simplicity of the system, we are hopeful that it will be able to make it easier for other labs to use and to integrate SRM with their advanced *in-vitro* models, which has until now been a major limiting factor with the techniques that can be used with such platforms.

**Funding.** Michael J. Fox Foundation for Parkinson's Research (MJFF-022407); National Institutes of Health (1R21AG074846-01A1); BrightFucos (A2022029S); The Zimmin Foundation; Förderkreis für Zusammenarbeit zwischen den Universitäten Konstanz und Tel Aviv; Teva Pharmaceutical Industries; The Aufzien Family Center for the Prevention and Treatment of Parkinson's Disease at Tel Aviv University; BioChip; Ministry of Science, Technology and Space (1001576154, 3-17351); European Research Council (851765); Israel Science Foundation (1934/23, 2141/20, 2248/19).

**Acknowledgment.** We are especially grateful to the funding agencies that supported this work. Israel Science Foundation (ISF grant: 2248/19, 1934/23), ERC SweetBrain 851765, The Aufzien Family Center for the Prevention and Treatment of Parkinson's Disease at Tel Aviv University and Israel Ministry of Science and Technology (Grant No. 3-17351), BioChip and TEVA (to B.M.M.). In addition, we would like to thank: “Förderkreis für Zusammenarbeit zwischen den Universitäten Konstanz und Tel Aviv” for supporting RB. This research was also supported by the Ministry of Innovation, Science and Technology, Israel (1001576154), the Aufzien Family Center for the Prevention and Treatment of Parkinson's Disease at Tel Aviv University, the Zimmin Foundation, TEVA Pharmaceuticals, Israel Science Foundation (ISF grant: 2141/20), BrightFucos grant (A2022029S), NIH grant 1R21AG074846-01A1, and the Michael J. Fox

Foundation (MJFF-022407) (to U.A.). The European Union – NextGenerationEU under the Italian Ministry of University and Research (MUR) National Innovation Ecosystem (grant ECS00000041 - VITALITY - CUP H33C22000430006) (to R.R).

**Disclosures.** The authors declare no conflicts of interest.

**Data availability.** Data underlying the results presented in this paper are not publicly available at this time but may be obtained from the authors upon reasonable request.

**Supplemental document.** See [Supplement 1](#) for supporting content.

## References

1. R. Rauti, N. Renous, and B. M. Maoz, "Mimicking the brain extracellular matrix in vitro: a review of current methodologies and challenges," *Isr. J. Chem.* **60**(12), 1141–1151 (2020).
2. P. Nikolakopoulou, R. Rauti, D. Voulgaris, I. Shlomy, B. M. Maoz, and A. Herland, "Recent progress in translational engineered in vitro models of the central nervous system," *Brain* **143**(11), 3181–3213 (2020).
3. B. M. Maoz, "Brain-on-a-Chip: Characterizing the next generation of advanced in vitro platforms for modeling the central nervous system," *APL Bioeng.* **5**(3), 030902 (2021).
4. B. M. Maoz, A. Herland, O. Y. F. Henry, W. D. Leineweber, M. Yadid, J. Doyle, R. Mannix, V. J. Kujala, E. A. FitzGerald, K. K. Parker, and D. E. Ingber, "Organs-on-Chips with combined multi-electrode array and transepithelial electrical resistance measurement capabilities," *Lab Chip* **17**(13), 2294–2302 (2017).
5. N. Renous, M. D. Kiri, R. A. Barnea, R. Rauti, Y. Leichtmann-Bardoogo, and B. M. Maoz, "Spatial trans-epithelial electrical resistance (S-TEER) integrated in organs-on-chips," *Lab Chip* **22**(1), 71–79 (2022).
6. M. M. Modena, K. Chawla, P. M. Misun, and A. Hierlemann, "Smart cell culture systems: integration of sensors and actuators into microphysiological systems," *ACS Chem. Biol.* **13**(7), 1767–1784 (2018).
7. C. G. Galbraith and J. A. Galbraith, "Super-resolution microscopy at a glance," *J Cell Sci* **124**(10), 1607–1611 (2011).
8. A.H. Shaib, A.A. Chouaib, and V. Imani, *et al.*, "Expansion microscopy at one nanometer resolution,". bioRxiv, bioRxiv:2022.08.03.502284. (2022).
9. T. L. Liu, S. Upadhyayula, and D. E. Milkie, *et al.*, "Observing the cell in its native state: Imaging subcellular dynamics in multicellular organisms," *Science* **360**(6386), eaaq1392 (2018).
10. U. Birk, J. V. Hase, and C. Cremer, "Super-resolution microscopy with very large working distance by means of distributed aperture illumination," *Sci. Rep.* **7**(1), 3685 (2017).
11. S. H. Chu, L. L. Lo, R. L. Lai, T. Tony Yang, R. R. Weng, J. C. Liao, and N. T. Huang, "A microfluidic device for in situ fixation and super-resolved mechanosensation studies of primary cilia," *Biomicrofluidics* **13**(1), 14105 (2019).
12. J. Tam, G. A. Cordier, Š Bálint, A. Sandoval Álvarez, J. S. Borbely, and M. Lakadamyali, "A microfluidic platform for correlative live-cell and super-resolution microscopy," *PLoS One* **9**(12), e115512 (2014).
13. B. Buchroithner, S. Mayr, F. Hauser, E. Priglinger, H. Stangl, A. R. Santa-Maria, M. A. Deli, A. Der, T. A. Klar, M. Axmann, D. Sivun, M. Mairhofer, and J. Jacak, "Dual channel microfluidics for mimicking the blood–brain barrier," *ACS Nano* **15**(2), 2984–2993 (2021).
14. R. Maraspini, C. H. Wang, and A. Honigmann, "Optimization of 2D and 3D cell culture to study membrane organization with STED microscopy," *J. Phys. D: Appl. Phys.* **53**(1), 014001 (2020).
15. Y. Ren, M. J. Mlodzianoski, A. C. Lee, F. Huang, and D. M. Suter, "A low-cost microwell device for high-resolution imaging of neurite outgrowth in 3D," *J. Neural Eng.* **15**(3), 035001 (2018).
16. W. Zhang, J. A. DeMattia, H. Song, and W. T. Couldwell, "Communication between malignant glioma cells and vascular endothelial cells through gap junctions," *J Neurosurg.* **98**(4), 846–853 (2003).
17. R. Dermietzel and D. C. Spray, "Gap junctions in the brain: where, what type, how many and why?" *Trends Neurosci.* **16**(5), 186–192 (1993).
18. N. N. Khodarev, J. Yu, E. Labay, T. Darga, C. K. Brown, H. J. Mauceri, R. Yassari, N. Gupta, and R. R. Weichselbaum, "Tumour-endothelium interactions in co-culture: coordinated changes of gene expression profiles and phenotypic properties of endothelial cells," *J Cell Sci.* **116**(6), 1013–1022 (2003).
19. I. K. Zervantonakis, C. R. Kothapalli, S. Chung, R. Sudo, and R. D. Kamm, "Microfluidic devices for studying heterotypic cell-cell interactions and tissue specimen cultures under controlled microenvironments," *Biomicrofluidics* **5**(1), 13406 (2011).
20. J. A. Joyce and J. W. Pollard, "Microenvironmental regulation of metastasis," *Nat. Rev. Cancer* **9**(4), 239–252 (2009).
21. A. C. Luca, S. Mersch, R. Deenen, S. Schmidt, I. Messner, K. L. Schäfer, S. E. Baldus, W. Huckenbeck, R. P. Piekorz, W. T. Knoefel, A. Krieg, and N. H. Stoecklein, "Impact of the 3D microenvironment on phenotype, gene expression, and EGFR inhibition of colorectal cancer cell lines," *PLoS One* **8**(3), e59689 (2013).
22. R. Rauti, A. Ess, B. Le Roi, Y. Kreinin, M. Epshtein, N. Korin, and B. M. Maoz, "Transforming a well into a chip: A modular 3D-printed microfluidic chip," *APL Bioeng.* **5**(2), 026103 (2021).
23. <https://guide.vutara.bruker.com/m/11201/122590-vutara-filter-sets>.
24. A. Tahmasbi, E. S. Ward, and R. J. Ober, "Determination of localization accuracy based on experimentally acquired image sets: applications to single molecule microscopy," *Opt. Express* **23**(6), 7630 (2015).
25. J. Chao, S. Ram, E. S. Ward, and R. J. Ober, "Investigating the usage of point spread functions in point source and microsphere localization," *Proc. SPIE Int. Soc. Opt. Eng.* **9713**, 97131M (2016).

26. R. J. Ober, S. Ram, and E. S. Ward, "Localization accuracy in single-molecule microscopy," *Biophys. J.* **86**(2), 1185–1200 (2004).
27. J. Chao, E. S. Ward, and R. J. Ober, "Fisher information theory for parameter estimation in single molecule microscopy: tutorial," *J. Opt. Soc. Am. A* **33**(7), B36–57 (2016).
28. [https://d3pcsg2wj9izr.cloudfront.net/files/42300/download/442472/Vutara350\\_B2004-RevA0\\_brochure.pdf](https://d3pcsg2wj9izr.cloudfront.net/files/42300/download/442472/Vutara350_B2004-RevA0_brochure.pdf).
29. B. Campello, J.G. Ricardo, D. Moulavi, and J. Sander, "Density-based clustering based on hierarchical density estimates," In: *Pacific-Asia Conference on Knowledge Discovery and Data Mining* (Springer, Berlin, Heidelberg, 2013), pp. 160–172.
30. [https://hdbscan.readthedocs.io/en/latest/parameter\\_selection.html](https://hdbscan.readthedocs.io/en/latest/parameter_selection.html).
31. A. B. Bloom and M. H. Zaman, "Influence of the microenvironment on cell fate determination and migration," *Physiol Genomics*. **46**(9), 309–314 (2014).
32. M. Kotini, E. H. Barriga, J. Leslie, M. Gentzel, V. Rauschenberger, A. Schambony, and R. Mayor, "Gap junction protein Connexin-43 is a direct transcriptional regulator of N-cadherin in vivo," *Nat. Commun.* **9**(1), 3846 (2018).
33. Y. Shi, X. Li, and J. Yang, "Cx43 upregulation in HUVECs under stretch via TGF- $\beta$ 1 and cytoskeletal network," *Open Med.* **17**(1), 463–474 (2022).
34. K. Piowarczyk, M. Paw, D. Ryszawy, M. Rutkowska-Zapała, Z. Madeja, M. Siedlar, and J. Czyż, "Connexin43high prostate cancer cells induce endothelial connexin43 up-regulation through the activation of intercellular ERK1/2-dependent signaling axis," *Eur. J. Cell Biol.* **96**(4), 337–346 (2017).
35. N. G. Avci, Y. Fan, A. Dragomir, Y. M. Akay, and M. Akay, "Investigating the influence of HUVECs in the formation of glioblastoma spheroids in high-throughput three-dimensional microwells," *IEEE Trans Nanobioscience* **14**(7), 790–796 (2015).
36. D. Thuringer, K. Berthenet, L. Cronier, E. Solary, and E. C. Garrido, "Primary tumor- and metastasis-derived colon cancer cells differently modulate connexin expression and function in human capillary endothelial cells," *Oncotarget* **6**(30), 28800–28815 (2015).